Monthly Notices of the ROYAL ASTRONOMICAL SOCIETY

MNRAS **505,** 582–592 (2021) doi:10.1093/mnras/stab1316
Advance Access publication 2021 May 10

Modelling of atmospheric optical turbulence with the Weather Research and Forecasting model at the Ali observatory, Tibet

Xuan Qian ,[1]★ Yongqiang Yao,[1] Lei Zou,[2]★ Hongshuai Wang,[3]★ Jia Yin[1,4] and Yao Li[1,4]

[1]*National Astronomical Observatories of China, Chinese Academy of Sciences, 20A Datun Road, Chaoyang District, Beijing, China*
[2]*Key Laboratory of Water Cycle and Related Land Surface Processes, Institute of Geographic Sciences and Natural Resources Research, Chinese Academy of Sciences, 11 Datun Road, Chaoyang District, Beijing, 100101, China*
[3]*Kaiyang Space Technology Co. LTD, 8 Malianwa North Road, Haidian District, Beijing, 100085, China*
[4]*University of Chinese Academy of Sciences, 19A Yuquan Road, Shijingshan District, Beijing, China*

Accepted 2021 April 30. Received 2021 April 23; in original form 2021 February 8

ABSTRACT

In this study, we make use of a meso-scale numerical model to obtain the parameters of atmospheric optical turbulence at the Ali observatory above the Tibetan Plateau. These parameters are essential for ground-based optical observations and some adaptive optics techniques. We present the characterization of the vertical distributions of atmospheric optical turbulence C_n^2 and the main integral parameters, such as coherence time τ_0, isoplanatic angle θ_0 and seeing ε_0 derived from C_n^2. Meanwhile, the measurement of C_n^2 obtained with a radiosonde instrument is used to quantify the model performance on reconstructing the optical turbulence above the site. This shows a high level of agreement and provides a reliable tool for astronomical site testing. The results presented in this paper demonstrate the good behaviour of the atmospheric optical turbulence condition at Ali, particularly during the summer half of the year. We find yearly median values of seeing $\varepsilon_0 = 0.47$ arcsec, isoplanatic angle $\theta_0 = 4.35$ arcsec and atmospheric coherence time $\tau_0 = 5.52$ ms in 2016, and we also provide independent confirmation of the potential of the Ali site in adaptive optics. Moreover, it has been proven that meso-scale models can provide reliable estimations of atmospheric optical turbulence conditions above an astronomical site on the Tibetan Plateau.

Key words: turbulence – atmospheric effects – methods: numerical – site testing.

1 INTRODUCTION

Atmospheric optical turbulence is a key parameter for evaluating astronomical observatories. It affects the imaging quality of telescopes and the photoconductive accuracy (Fried 1966; Liu et al. 2013), and it also affects the stability of the optical communication system in free space (Li, Wu & Hou 2012). The resolving power and imaging quality of ground-based telescopes depend on the intensity of optical turbulence. The adaptive optical system is an essential installation for a large ground-based telescope as it compensates for the effects of optical turbulence, and also makes the imaging resolution of the telescope close to the diffraction limit (Fried 1982; Hickson 2014). For the rational design and efficient operation of an adaptive optical system, it is necessary to know the characteristics of optical turbulence, especially for wide field adaptive optics (WFAO) systems, such as laser tomography adaptive optics (LTAO), ground-layer adaptive optics (GLAO), multi-object adaptive optics (MOAO) and multi-conjugated adaptive optics (MCAO). So, it is fundamental to obtain the characteristics of optical turbulence in the atmosphere above an observatory site.

The main parameters for characterizing optical turbulence at a site are the refractive index structure constant C_n^2, the atmospheric coherence length r_0, the atmospheric coherence time τ_0, seeing ε, the isoplanatic angle θ_0, the scintillation index σ_I^2, etc. (Masciadri, Vernin & Bougeault 1999). A variety of mature devices have been developed to measure these parameters, such as the Multi-Aperture Scintillation Sensor (MASS), the Differential Image Motion Monitor (DIMM), the Surface layer NOn-Doppler Acoustic Radar (SNODAR), the Scintillation Detection and Ranging (SCIDAR), radiosoundings, etc. (Sarazin 1997; Li et al. 2012; Wang et al. 2012). Generally, the actual measurement involves obtaining the data on an optical path, which is insufficient to evaluate the characteristics of optical turbulence above a site. Moreover, as large telescopes are expensive, and the competition when applying for observation time is fierce, there is a great demand to optimize the telescope's observation schedule according to different observation conditions, in order to improve the efficient use of telescopes (Sarazin 1997). Based on the requirements mentioned above, the international astronomical community has gradually developed the modelling method of using meteorological parameters to compute the parameters of atmospheric turbulence.

By using meso-scale atmospheric numerical models to calculate meteorological parameters, the vertical optical turbulence C_n^2 can be obtained, and the integral parameters (seeing, isoplanatic angle, coherence time, etc.) can be derived by the relationship between

★ E-mail: qianxuan@nao.cas.cn (XQ); zoulei@igsnrr.ac.cn (LZ); wanghs@nao.cas.cn (HW)

meteorological parameters and optical turbulence (i.e., the modelling method of optical turbulence). From the models, we can derive the spatial and temporal distributions of optical turbulence parameters, within a distance of a few metres to a few tens of kilometres and a time-span of a few minutes to decades. This can help us identify the optimizing area of atmospheric optical turbulence condition, it can greatly reduce the work intensity and cost of the field reconnaissance for the surveys of astronomical sites, and it can also improve the work efficiency. Furthermore, the optical turbulence condition can be forecast in future, which can help to optimize the observation schedule of telescopes, and provide the optimum working time for telescope observations, adaptive optics, applications in optical engineering, optoelectronic equipments designed for atmospheric optical transmission, etc.

At the present stage, the methods for using meso-scale numerical models such as Meso-NH, the fifth-generation Penn State/NCAR Meso-scale Model (MM5), the European Center for Medium-Range Weather Forecasts (ECMWF), the Weather Research and Forecasting (WRF), etc., to obtain optical turbulence have been applied and validated at many observatories (Masciadri et al. 1999; Masciadri, Vernin & Bougeault 2001; Cherubini, Businger & Lyman 2008; Lascaux, Masciadri & Hagelin 2011; Giordano et al. 2013; Turchi, Masciadri & Fini 2017; Osborn & Sarazin 2018). For the MOdelling ESO Sites (MOSE) project, the non-hydrostatic Meso-NH model has been used, which can provide three-dimensional distributions of atmospheric flow and optical turbulence with suitable vertical resolutions, and can be applied in adaptive optics (Masciadri et al. 1999; Masciadri 2003, 2006; Masciadri, Lascaux & Fini 2013; Lascaux et al. 2011; Turchi et al. 2017; Masciadri, Martelloni & Turchi 2020). At the Mauna Kea Weather Center, the MM5 has been introduced to provide forecasts of atmospheric parameters, with a horizontal resolution of 1 km (Cherubini et al. 2008), which is a regional meso-scale model for climate projections and weather forecasts. Meanwhile, a mature prediction system of optical turbulence has been established, which is mainly responsible for providing forecasts of meteorological parameters and optical turbulence parameters for the observatory. Experimental work on model forecasting in the Canary Islands is also being carried out (Businger & Cherubini 2011; Hagelin, Masciadri & Lascaux 2011). At Cerro Paranal, Osborn & Sarazin (2018) have used the dynamical ECMWF model to forecast the temporal evolutions of the dominating features for the wide-field adaptive optics system, and the ECMWF is a global forecasting model for the mid-latitudes. Giordano et al. (2013, 2014) have made use of the meso-scale regional WRF model to forecast atmospheric parameters at the Roque de Los Muchachos (ORM), as well as to validate the model performance. Masciadri et al. (2001) and Trinquet & Vernin (2007) have presented numerical and analytical models for calculating optical turbulence parameters, by comparing with the measured data; the accuracy of the results from the models and those from actual measurements is comparative (Masciadri 2006; Sivo et al. 2018; Masciadri et al. 2020). Moreover, it has been proven that meso-scale models can provide better computation of meteorological parameters with high resolution above mid-latitude astronomical sites (Masciadri 2003, 2006; Masciadri et al. 2013; Basu et al. 2020). The modelling method for obtaining the characteristics of atmospheric turbulence has been widely used at many observatories, as well as in the fields of atmospheric optical transmission engineering (Wang, Yao & Liu 2013), and it has been proven to be a feasible method with high precision (Bougeault, De Hui & Fleury 1995; Cherubini et al. 2008; Lascaux, Masciadri & Hagelin 2009; Liu et al. 2010).

Figure 1. The current construction of the Ali site, mainly the ridge A (Ali-A).

The Ali observatory is a candidate site for the Chinese Large Optical Telescope Project, which is located at (32°.30 N, 80°.05 E), 5050 m above sea level, in the south-west area of the Tibetan Plateau. Fig. 1 shows the current construction of the Ali site, mainly the ridge A at an altitude of 5050 m (Ali-A). As for the adaptive optical systems designed for the large ground-based optical telescope, we need to obtain the characteristics of the optical turbulence conditions above the site, especially the vertical distribution of the refractive index structure constant C_n^2, which is of great significance. The turbulence at the ground layer at Ali has been found to be remarkably weak and relatively thin using lunar scintillometer observations (Hickson et al. 2020). In this paper, we examine the possibility of characterizing the optical turbulence in the whole atmosphere by using the meso-scale meteorological WRF model, which has been used at other sites (Trinquet & Vernin 2007; Kemp, Felton & Allis 2008; Ye 2011; Giordano et al. 2013; Basu et al. 2020). The WRF model can obtain the synoptic scale phenomena from global weather forecast systems. It uses a set of physical schemes to obtain meso-scale variations in the atmosphere, typically down to the order of 1 km, as processes on smaller scales are handled with subgrid parametrizations. Meanwhile, the source code and the model are completely open source, and can be downloaded and used for free. In previous work (Qian et al. 2020a, b), we have used this numerical model to derive the characteristics of high-altitude wind and precipitable water vapour at Ali, and we have shown that the meso-scale numerical WRF model can provide reliable computations of atmospheric parameters over the Tibetan Plateau.

The goal of this paper is to obtain the optical turbulence condition in the whole atmosphere above the Ali observatory, using the WRF model. We study the ability of the WRF model to assess the atmospheric optical turbulence condition in the complicated terrain area on the Tibetan Plateau. As a reference, we introduce the atmospheric optical turbulence parameters derived from the radiosonde measurement located at the Ali Radiosonde Station, about 25 km north to the site. We also present a climatological characterization of atmospheric optical parameters on the time-scale of 1 yr at the Ali site.

In Section 2, we briefly describe the WRF model and the available data from measurements. The results of the atmospheric optical turbulence parameters during the whole night obtained from model

Table 1. The WRF model configuration. ΔX is the horizontal resolution of each imbricated domain, and the last column gives the time intervals of the computations.

Domain	ΔX (km)	Grid points	Domain size (km)	Time interval (s)
d 01	9.0	201 × 101	2500 × 2500	60
d 02	3.0	101 × 101	500 × 500	60
d 03	1.0	101 × 201	200 × 200	30

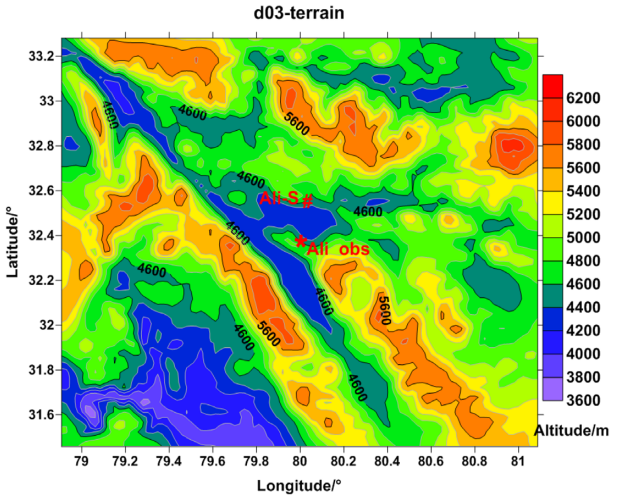

Figure 2. The topographic area of domain 03 with a 1-km resolution, and the domain size is 200 × 200 km^2, centred at the Ali observatory. The symbols '∗' and '#' in red indicate the locations of the Ali observatory (Ali-obs) and the Ali radiosonde station (Ali-S). The colour bar indicates the altitude (Qian et al. 2020a, b).

are given in Section 3. The main conclusions are summarized in Section 4.

2 MODEL CONFIGURATION AND MEASUREMENT

The meso-scale numerical WRF model is a completely compressible non-hydrostatic model, and also a weather prediction system for atmospheric research. In the horizontal direction, the Arakawa C grid points are applied, and the terrain is represented by mass coordinates in the vertical direction; in terms of time integral, the third- or fourth- order Runge–Kutta algorithm is adopted. The source data, the required terrain and weather data for the WRF model configuration are freely available at the National Center for Atmospheric Research (NCAR) and National Centers for Environmental Prediction (NCEP) web sites. Using the meso-scale model, the analysis results with high resolution can be derived through the model running accurate physical schemes, which can provide effective assessments of astronomical sites.

In this study, the specific design of the WRF model configuration is as follows (Qian et al. 2020a, b). The model runs in three imbricated domains of grid-nesting mode with different resolutions (9, 3 and 1 km), as shown in Table 1. These three domains are all centred at the Ali observatory (80.°08 E, 32.°30 N; 5050 m above sea level). In the vertical direction, simulations are provided at 34 levels (from the ground up to the 20 hPa pressure level), represented by Sigma coordinates. When the model starts running, grid nudging is carried out in the outer domain for humidity (q), wind (u/v) and temperature (t), ensuring that the atmospheric conditions on a large scale in the model are very close to the actual conditions, so the accuracy and reliability of the model results can be improved.

The Tibetan Plateau is the highest plateau in the world with complex terrain, and the Ali observatory is established in the south-west of the plateau. As the characteristics of the planetary boundary layer above the plateau are distinctive, the terrestrial data are interpolated to fit the simulated domains. For the boundary and initial conditions, we make use of the public ERA-Interim data that are available from the ECWMF. These data sets are of a horizontal resolution of 0.°75 × 0.°75, and can be available at Beijing Time (BT) 00:00 (UTC 18:00), BT 06:00 (UTC 00:00), BT 12:00 (UTC 06:00) and BT 18:00 (utc 12:00) every day.

Based on the specific meteorological, topographical and environmental conditions on the Tibetan Plateau, the physical schemes used for the model configuration at Ali in this study are as follows.

(i) The WSM6 cloud scheme (WRF single-moment six-class) is used for the microphysics scheme.
(ii) The Grell–Devenyi (GD) scheme is used for the convective scheme.
(iii) The NOAH land-surface model is used.
(iv) The short-wave radiation uses the Dudhia scheme, and for the long-wave radiation, the rapid radiative transfer model (RRTM) scheme is used.
(v) For the planetary boundary layer, the Mellor–Yamada–Janjic (MYJ) scheme is adopted.

All simulations performed with WRF start running at BT 18:00 (UTC 12:00) the day before, and last for 30 h. The first 6 h is the spin-up time of the model running, which is rejected; therefore, we take into account the model outputs starting at BT 00:00 (UTC 18:00) each day.

In this paper, we present the simulation results of domain 03 in 2016 above the Ali observatory, with the highest horizontal resolution of 1 km, close to the scale of atmospheric optical turbulence (Giordano et al. 2013). The time resolution is 0.5 h, with 34 vertical levels (from the ground to 20 hPa pressure level), and the coverage of this domain is 200 × 200 km^2. Fig. 2 shows the topographic area of domain 03 with a 1-km resolution (Qian et al. 2020a, b). The red symbols '#' and '∗' indicate the locations of Ali-S (Ali radiosonde station, 80.°08 E, 32.°50 N, at 4280 m) and the Ali observatory (Ali-obs), respectively.

The Ali radiosonde station is about 25 km north of the Ali site, managed by the Ali Meteorological Bureau, and the altitude is about 4280 m above sea level (Qian et al. 2018, 2020a). It is worth mentioning that the radiosonde observations are performed at BT 07:00 (UTC 23:00) in the morning and 19:00 (UTC 13:00) in the evening each day, and one more time at BT 13:00 (UTC 05:00) at noon in summer (June–August). In 2016, the effective data rate was up to 87 per cent, and most of the missing data were at BT 07:00 in April and July. As there is a time difference of 2.5 h between Ali and Beijing, BT 07:00 at Ali is still at night most days during 2016. In this study, we introduce the radiosounding results of optical turbulence at BT 07:00 for reference.

3 RESULTS

The WRF model outputs the profiles of temperature, wind and other physical parameters. From the vertical potential temperature gradient and the vertical wind shear, we can retrieve the vertical profiles of optical turbulence C_n^2 using the Trinquet–Vernin parametrization (Trinquet & Vernin 2007). The results of three major integral

atmospheric turbulence parameters (seeing ε_0, coherence time τ_0 and isoplanatic angle θ_0) are computed. According to the astronomical twilight in 2016 at Ali (i.e. the times corresponding to astronomical dawn and astronomical dusk are the beginning and end of astronomical night), the results of atmospheric optical turbulence parameters during the whole night are presented. As the radiosonde observations are performed at Ali-S, the analysis of simulated versus observed results at Ali-S are introduced as a reference. When discussing the results, in the solar year there are two periods: the summer half of the year (from April to September) and the winter half of the year (from October to March). The results of the optical turbulence parameters in different seasons are investigated.

3.1 C_n^2 Profile

Because of the effect of atmospheric optical turbulence, the imaging quality of ground-based telescopes can be affected severely at the time of observation, and the resolution that the telescope can achieve is reduced with respect to the theoretical diffraction limit. In 1941, Kolmogorov developed a statistical theory of turbulence based on the Richardson cascade model by using dimensional analysis, stating that the energy is transferred step-by-step between different scales in the turbulence, from the turbulent eddy on a large scale to that on a small scale (Kolmogorov 1941). When the injection and dissipation of energy are in equilibrium, the transmission of energy reaches a state of dynamic stability. Between the inner and outer scales of turbulence, there is an inertial area. In this area, the turbulence is isotropic, and the structural function of wind speed is only related to the rate and distance of the energy dissipation. As there is a gradient in the vertical direction, the temperature is not isotropic, and is usually replaced by the potential temperature. The potential temperature can be considered as a conserved quantity in the dry adiabatic process, which is defined as the temperature a dry air parcel would have if restored adiabatically from the existing state to a standard pressure of 1000 hPa:

$$\theta = T\left(\frac{1000}{P}\right)^{0.286}. \tag{1}$$

Here, θ is the potential temperature, T is the temperature and P is the pressure.

The temperature fluctuation structure constant C_t^2 can be determined by the wind shear and the potential temperature gradient:

$$C_t^2 = \langle C_t^2\rangle_{\rm m}\frac{\chi}{\langle\chi\rangle_{\rm m}}\left(\frac{S}{\langle S\rangle_{\rm m}}\right)^{1/2}; \tag{2}$$

$$\chi = \frac{{\rm d}\theta}{{\rm d}z}; \tag{3}$$

$$S = \sqrt{\left(\frac{{\rm d}V_x}{{\rm d}z}\right)^2 + \left(\frac{{\rm d}V_y}{{\rm d}z}\right)^2}. \tag{4}$$

Here, S is the wind shear, χ is the gradient of potential temperature, Vx and Vy are the horizontal and vertical wind speeds, respectively, and $\langle\rangle_{\rm m}$ indicates the median values of all observations at the same altitude.

The atmospheric refractive index is a passive conservative quantity, similar to the potential temperature structure constant, and there is a refractive index structure parameter, with which the relation is (Businger & Cherubini 2011)

$$C_n^2 = \left(\frac{80\times10^{-6}p}{t^2}\right)^2 C_t^2. \tag{5}$$

Here, C_n^2 is the intensity of atmospheric optical turbulence. The vertical distribution of C_n^2 is the atmospheric optical turbulence profile, denoted as the C_n^2 profile.

The characteristic of the C_n^2 profile determines the number of turbulent layers required for the tomographic reconstruction in real-time calculations, and the corresponding capacity of computation is required. In multi-layered conjugate adaptive optics (i.e. MCAO) systems, the number of deformable mirrors and the optimum coupling degree are determined by the C_n^2 profile. A good C_n^2 profile can simulate and determine the potential efficiency of a GLAO system, and can also make the reconstruction algorithm before scientific observations converge quickly.

Figs 3 and 4 show the mean and median C_n^2 profiles during the whole night obtained from model and radiosonde observations at Ali-S and Ali-A in 2016, as well as the profiles in the summer half-year and those in the winter half-year. Weak turbulence occurs in the summer half-year, while the turbulence is slightly stronger during the winter half-year. From the C_n^2 profiles in 2016, below about 7 km above sea level, the agreement between the shapes of the C_n^2 profiles derived from the model and radiosoundings is good, and the model could reconstruct the C_n^2 profiles near the ground. In general, the variations of the C_n^2 profiles are relatively consistent, as higher than 7 km above sea level, especially at about 12–13 km above sea level (i.e. corresponding to the height of tropopause in the jet-stream region), the C_n^2 values simulated from model are slightly smaller than the observed results. The vertical distributions of C_n^2 in the winter half-year are very well described by the WRF model, and below about 11 km above sea level, the model results are slightly overestimated compared with the measured results. However, in the summer half-year, on the whole, the numerical model appears to have slightly underestimated C_n^2. It should be noted that the slight underestimation occurring during the summer half-year could be because the observed sample is not rich in these months, as most of the samples at BT 07:00 from radiosonde observations are missing.

Fig. 5 displays the temporal variation of daily median C_n^2 profiles in the night from the model. Figs 6 and 7 present the yearly and monthly quartiles of the C_n^2 profiles at night obtained from model during 2016 at the Ali site. On the whole, C_n^2 decreases with height, especially at the ground surface layer, where it decreases greatly with height within 1 km above the ground. Between 6 and 8 km above sea level, the C_n^2 values increase slightly and still decrease obviously at the tropopause (about 12–13 km above sea level at Ali). Large C_n^2 values appear in the winter half-year, while small C_n^2 values prevail during the summer half-year, which corresponds to the influence of the 200-hPa high-altitude wind field (Qian et al. 2020a). In different seasons, the turbulence varies obviously near the ground surface layer as well as at the tropopause. In 2016, the mean variation range of the C_n^2 profiles is between $10^{-19.5}$ and $10^{-13.5}$ m$^{-2/3}$.

3.2 Seeing ε_0

The atmospheric seeing ε_0 represents the full width at half-maximum (FWHM) of the point spread function (PSF), the best angular resolution that an optical telescope can achieve in a long exposure image, corresponding to the FWHM of the blurry blob when observing a star through the atmosphere. For a site survey on classical telescopes without adaptive optical terminals, ε_0 is one of the main considerations, as the adaptive optics can improve the imaging quality by compensating for the wavefront distortion caused by atmospheric disturbance in real time. The ε_0 can affect the number of actuators required for the deformable mirrors and the stroke of each

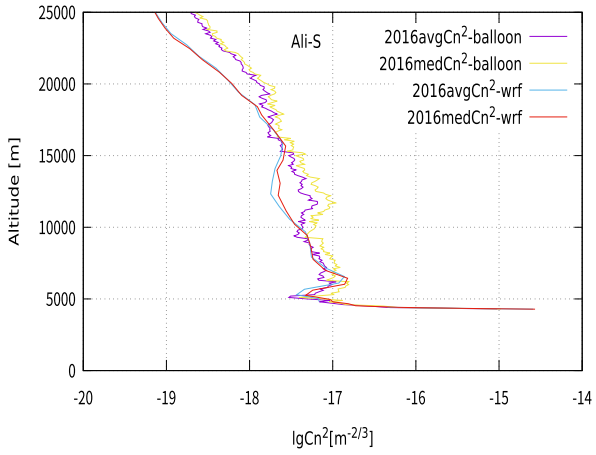

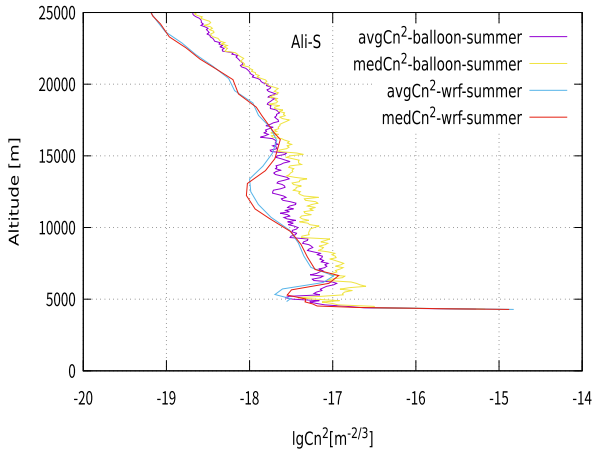

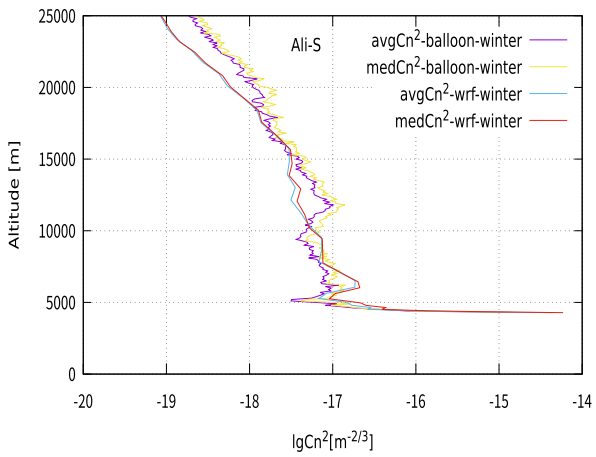

Figure 3. The median and mean C_n^2 profiles derived from the WRF model and radiosonde measurements at Ali-S. Top: the median and mean profiles for the total sample at night in 2016. Middle: the same for the sample during the summer half-year (from April to September). Bottom: the same for the sample in the winter half-year (from October to March). The purple and blue lines indicate the mean profiles, and the yellow and red lines indicate the median profiles.

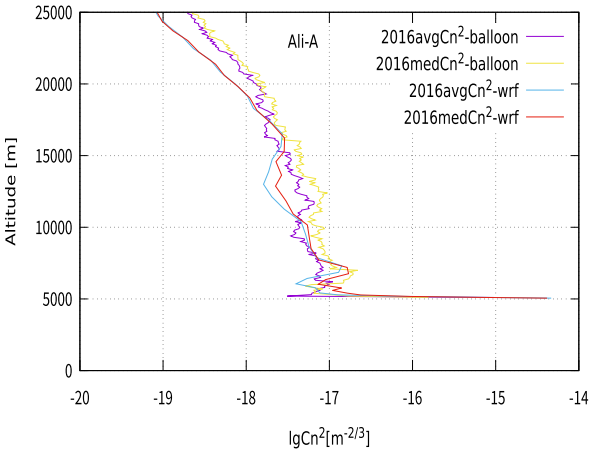

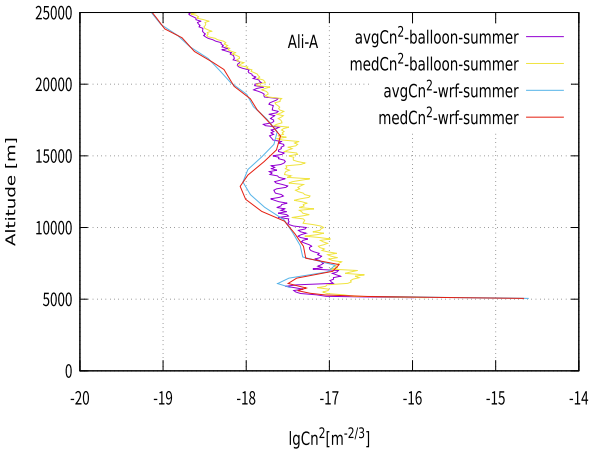

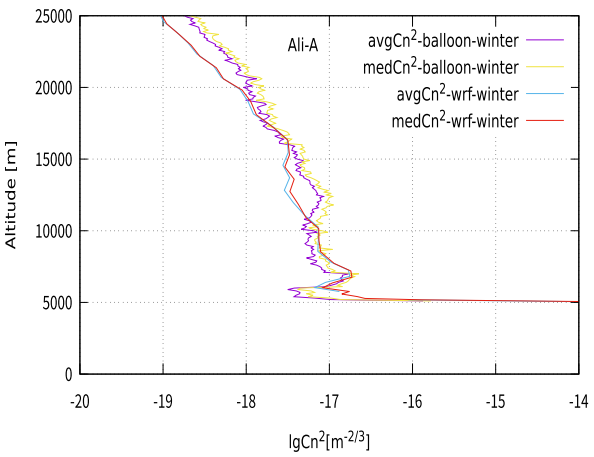

Figure 4. The median and mean C_n^2 profiles derived from the WRF model and radiosonde measurement at Ali-A. Top: the median and mean profiles for the total sample at night in 2016. Middle: the same for the sample during the summer half-year (from April to September). Bottom: the same for the sample in the winter half-year (from October to March). The purple and blue lines indicate the mean profiles, and the yellow and red lines indicate the median profiles.

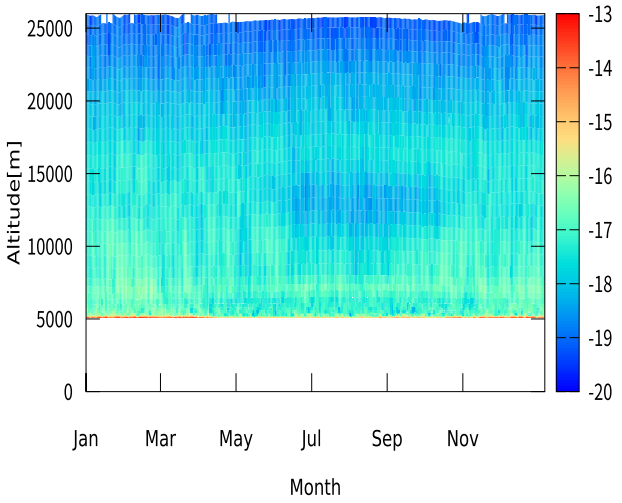

Figure 5. Temporal evolution of daily median C_n^2 profiles at night calculated using the WRF model in 2016. The colour bar indicates the $\lg C_n^2$ value, in units of $m^{-2/3}$.

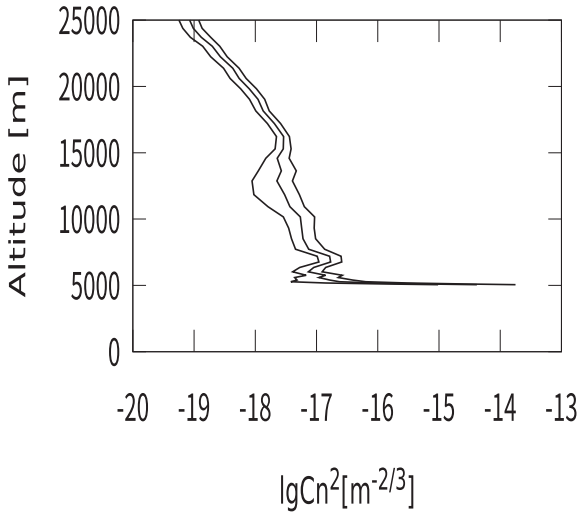

Figure 6. The yearly quartiles of the C_n^2 profiles at night calculated using the WRF model during 2016 at the Ali site.

actuator, the number of subpupils of the wavefront sensor, the power requirements for the laser guides, the area of the sky that reaches the specified image quality, and the computing power of the computer. Meanwhile, the variation of ε_0 with time can affect the updating speed and accuracy of the background work of the adaptive optical control loop. At the excellent observatories in the mid-latitude, the typical value of seeing ε_0 is usually 0.6–1.0 arcsec. The seeing ε_0 can be calculated as

$$\varepsilon_0 = 5.25\,\lambda^{(-1)/5}\left[\int C_n{}^2(h)\mathrm{d}h\right]^{3/5}, \tag{6}$$

where λ is the wavelength, p is the total air pressure, h is the altitude and t is the air temperature.

In the analysis, we make use of the statistical operators: the bias, the root-mean-squared error (rmse) and the sigma, which indicate the information of the statistical and systematic uncertainties, shown as follows:

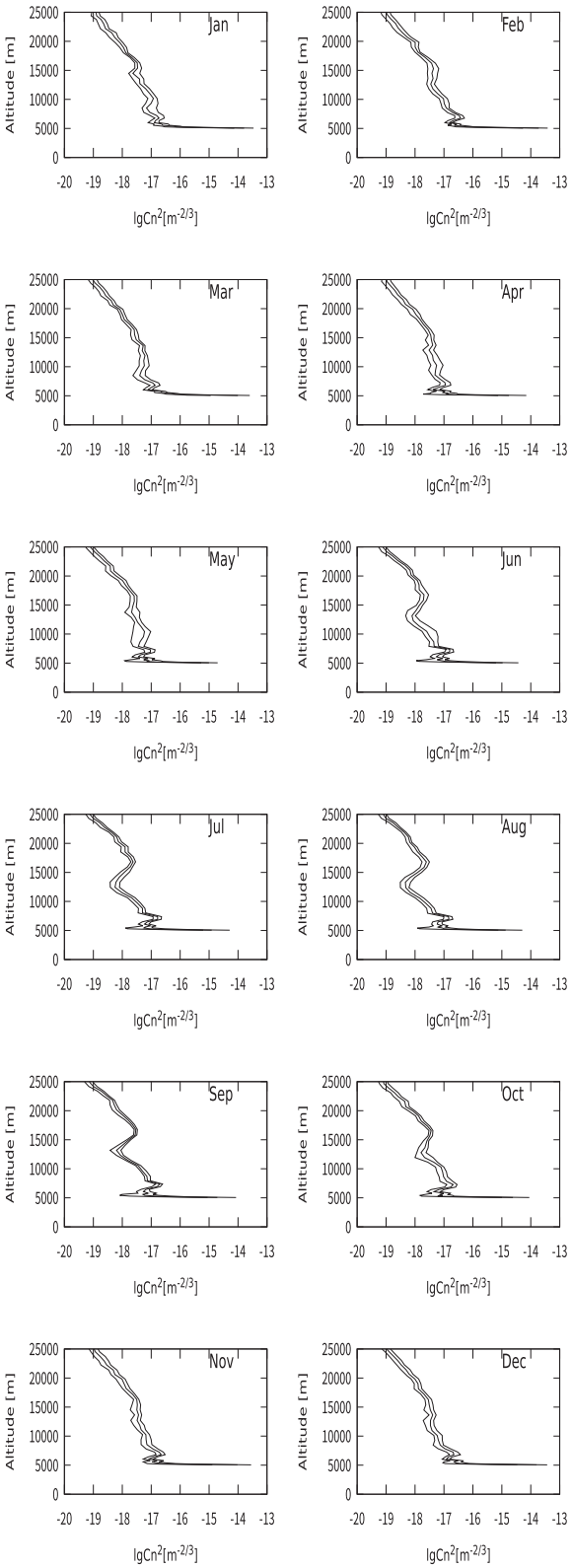

Figure 7. Monthly quartiles of the C_n^2 profiles in the night computed by the WRF model during 2016 at the Ali site.

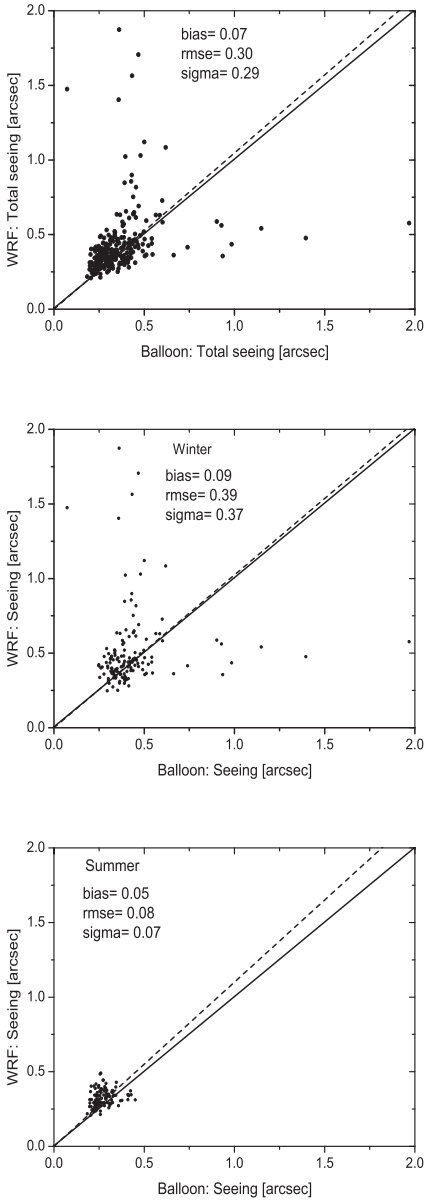

Figure 8. Scattered plots of the total seeing values during the whole of 2016 (top), the seeing results during the winter half-year (middle) and the summer half-year (bottom) comparing radiosonde measurements and model outputs obtained in the night at the Ali site.

$$\text{bias} = \sum_{i=1}^{N} \frac{(Y_i - X_i)}{N}; \tag{7}$$

$$\text{rmse} = \sqrt{\sum_{i=1}^{N} \frac{(Y_i - X_i)^2}{N}}; \tag{8}$$

$$\text{sigma} = \sqrt{\text{rmse}^2 - \text{bias}^2}. \tag{9}$$

Here, X_i denotes the results of individual observations, Y_i denotes the results of individual simulations at the same time (i), and N is the total number of samples.

Fig. 8 shows the scattered plots of the total seeing values during the whole of 2016 (top), the seeing results during the winter half-year (middle) and the summer half-year (bottom) comparing radiosonde measurements and model outputs obtained in the night at the Ali observatory. It can be observed that the model appears to be very much in agreement with the radiosonde measurements, with an almost negligible bias below 0.1 arcsec. Fig. 9 shows the cumulative probability distributions of seeing derived from the WRF model and radiosonde observations at the same time in the night at the Ali observatory. The quartile values of seeing obtained from the WRF model are in good agreement with the green lines representing the observed seeing values at Ali. As the observations are taken at Ali-S, the observed seeing results at Ali-A are directly integrated from 5050 m above sea level, and the integral values of about 800 m near the ground are omitted, which greatly contributes to the total seeing. At Ali-S, between the seeing values of 0.25 and 1.15 arcsec, the cumulative probabilities of seeing obtained from observations are slightly smaller than those from model. At Ali-A, the cumulative probabilities obtained from observations are slightly larger than those from model. The seeing values are below 0.3 arcsec for about 30 per cent and 20 per cent of the time in 2016 at Ali-S and Ali-A, respectively. The seeing values below 1.0 arcsec are above 95 per cent of such seeing integrations.

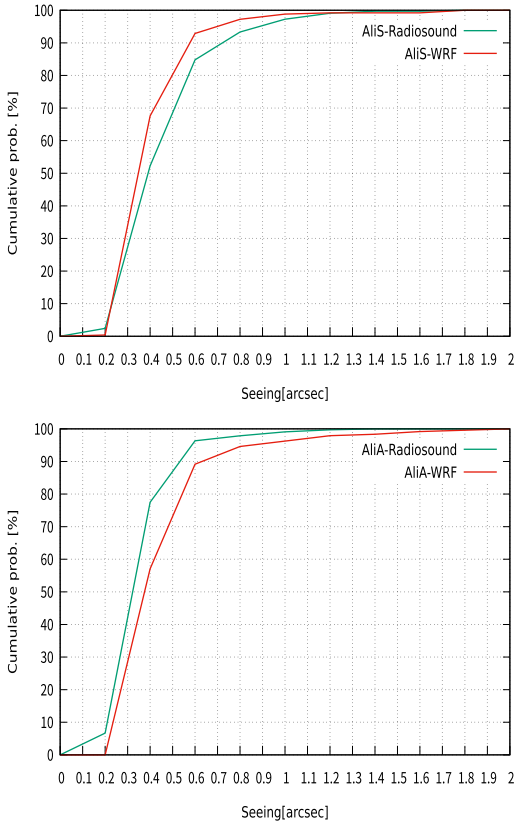

Figure 9. Cumulative probability distributions of seeing at night in 2016 at Ali, obtained from the radiosonde measurements (green line) and the WRF model (red line) simultaneously.

Fig. 10 shows the daily distribution of seeing during the whole night in 2016 at the Ali observatory. The seeing values vary between 0.2 and 1.5 arcsec, with large values of 0.4–1.5 arcsec appearing in the winter half-year, while small values in the range of 0.2–0.5 arcsec occur in the summer half-year. Table 2 presents the monthly and yearly median seeing values at night in 2016 at the Ali observatory. The yearly median seeing during the whole night is about 0.47 arcsec in 2016; in the summer half-year, the monthly median seeing values

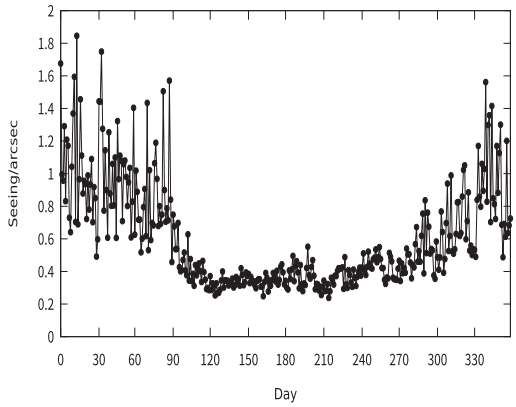

Figure 10. The daily distribution of seeing during the whole night in 2016 at the Ali observatory.

Table 2. The median values of seeing, coherence time and isoplanatic angle during the whole night obtained from model in 2016 at the Ali observatory.

Month	Seeing, ε_0 (arcsec)	Isoplanatic angle, θ_0 (arcsec)	Coherence time, τ_0 (ms)
Jan	0.72	3.39	2.61
Feb	0.80	3.20	1.54
Mar	0.67	3.76	3.11
Apr	0.34	3.71	3.64
May	0.31	4.11	5.95
Jun	0.31	5.00	10.67
Jul	0.30	5.06	11.41
Aug	0.31	5.63	14.85
Sep	0.36	4.67	7.83
Oct	0.42	3.79	3.45
Nov	0.50	3.66	2.51
Dec	0.68	3.71	2.14
Yearly	0.47	4.35	5.52

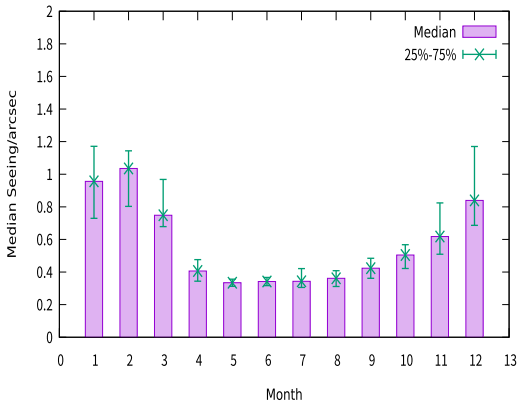

Figure 11. Monthly quartile values of seeing at night in 2016 at the Ali observatory, with the histograms showing median values, and the vertical bars indicating quartile values of seeing.

are all below 0.4 arcsec, while they are larger in the winter half-year, below 0.8 arcsec. Also, Fig. 11 shows the monthly quartiles of seeing during the whole night in 2016, with the vertical bars indicating the quartile values of seeing. On the whole, the small seeing at the Ali observatory is in line with that at the mid-latitude excellent observatories.

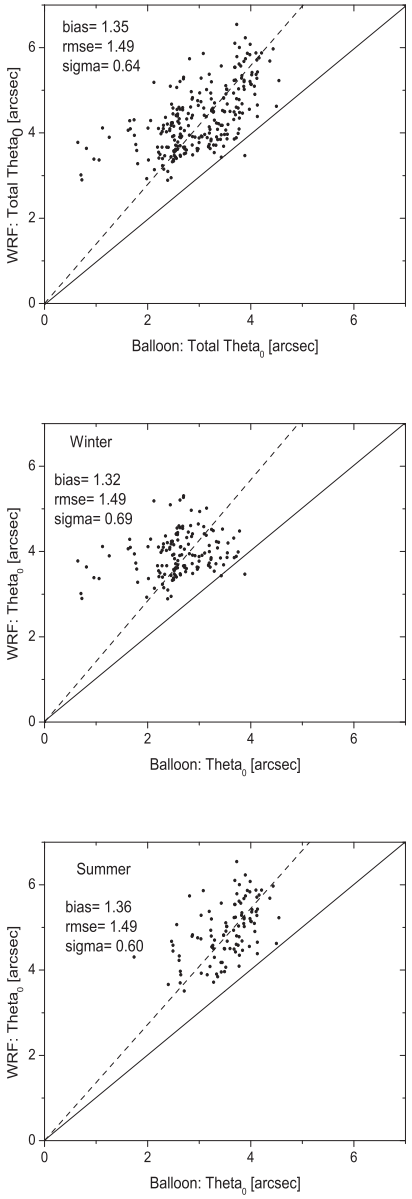

Figure 12. Scattered plots of the total θ_0 during the whole of 2016 (top), and θ_0 during the winter half-year (middle) and the summer half-year (bottom), comparing radiosonde measurements and model outputs at the Ali site.

3.3 Isoplanatic angle θ_0

The isoplanatic angle θ_0 depends on ${C_n}^2$, as follows:

$$\theta_0 = 0.058\lambda^{6/5}\left[\int h^{5/3}{C_n}^2(h)\,\mathrm{d}h\right]^{(-3)/5}. \quad (10)$$

Fig. 12 shows the scattered plots of the total θ_0 during the whole of 2016 (top), and θ_0 during the winter half-year (middle) and the summer half-year (bottom) comparing radiosonde measurements and model outputs obtained in the night at the Ali observatory. For the three samples in different time periods, there is a comparable value of sigma, 0.60–0.70 arcsec. For the bias and rmse, the values are similar in each time period; for the bias, the values are all around 1.35 arcsec, and the values of rmse are all 1.49 arcsec.

Fig. 13 shows the cumulative probability distribution of the θ_0 values at night, obtained from observations and the model at Ali. It

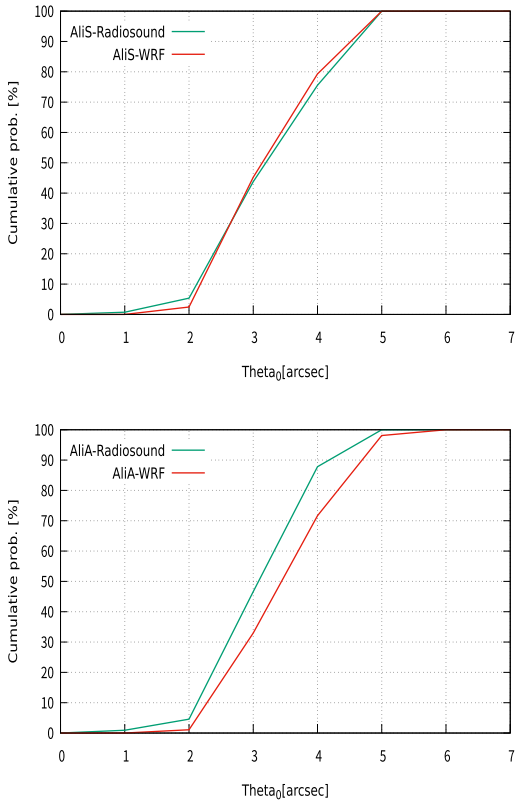

Figure 13. Cumulative probability distributions of the θ_0 values at night in 2016 at Ali, obtained from the radiosonde measurements (green line) and the WRF model (red line).

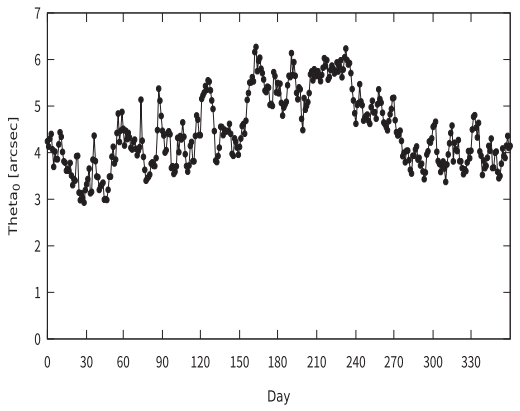

Figure 14. The daily distribution of θ_0 at night in 2016 at the Ali site, computed by the model.

can be concluded that the samples correspond well with the typical conditions of θ_0 at Ali, especially at Ali-S where the observations are undertaken. The θ_0 values are below 5 arcsec for about 100 per cent of the time. As the observation is performed at Ali-S, 4280 m above sea level, and the integral height of radiosonde observations at the Ali observatory (Ali-A) starts at 5050 m above sea level, the θ_0 values from observations are slightly larger than from the model; the θ_0 values are below 5 arcsec for more than 95 per cent of the time.

Fig. 14 displays the daily distribution of θ_0 at night in 2016 at the Ali observatory, and Table 2 and Fig. 15 show the quartile values of θ_0 at night, obtained from the WRF model. During 2016, the θ_0 values are between 3 and 6 arcsec. Large values of θ_0 occur in

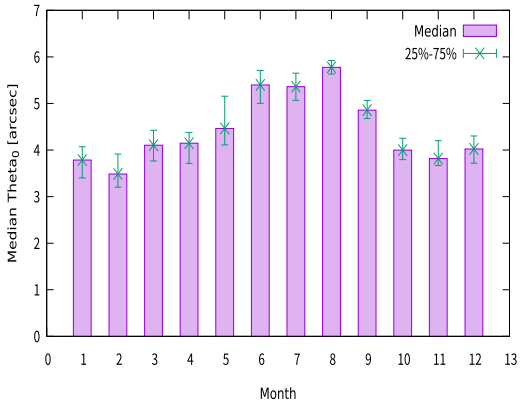

Figure 15. Quartiles of θ_0 at night in different seasons in 2016 at the Ali observatory, with the histograms showing the median values, and the vertical bars indicating quartile values of the θ_0.

summer while, in winter, the θ_0 values are small; the yearly median θ_0 is about 4.35 arcsec.

3.4 Coherence time τ_0

The coherence time depends on C_n^2 and the vertical profiles of wind speed:

$$\tau_0 = 0.058\,\lambda^{6/5}\left[\int |V(h)|^{5/3} C_n^2(h)\,\mathrm{d}h\right]^{(-3)/5}. \quad (11)$$

Fig. 16 shows the scattered plots of the total τ_0 during the whole of 2016 (top), and τ_0 during the winter half-year (middle) and the summer half-year (bottom), comparing radiosonde measurements and model outputs obtained in the night at the Ali observatory. It can be seen that there is a very good correlation between observations and model simulations. For the samples in each time period, the bias is small, and especially in the summer half-year there is an almost negligible bias; the rmse and sigma are about 1.20–2.00 ms. Fig. 17 shows the cumulative probability distributions of τ_0 at night in 2016 at the Ali observatory, obtained from radiosonde observations and the WRF model. The distribution of τ_0 from the model is basically in agreement with that from observations, as the observed τ_0 values are slightly larger than the simulated τ_0 results. The difference between observations and model calculations at Ali-S is slightly larger than at Ali-A.

Fig. 18 presents the daily distribution of τ_0 at night in 2016 at Ali, derived from the model. The τ_0 values are 1.00–26.00 ms in 2016; large values of τ_0 occur in summer (i.e. 10–26 ms), whereas, in winter, the τ_0 values are below 8.00 ms. Table 2 and Fig. 19 show the quartile values of τ_0 at night in 2016. The yearly median τ_0 is about 5.52 ms; in summer, the large τ_0 values are usually above 10.00 ms and, in winter, the τ_0 values are below 3.00 ms.

4 CONCLUSIONS

In this paper, we obtain the main characteristics of atmospheric optical turbulence during the whole astronomical night in 2016 at the Ali observatory on the west Tibetan Plateau. By using the meso-scale WRF model, coupled with the Trinquet–Vernin parametrization, we present the statistics of the C_n^2 profiles and the main integral parameters, such as isoplanatic angle θ_0, seeing ε_0 and coherence time τ_0, as well as their seasonal trends. Because a direct way of retrieving atmospheric parameters is to use radiosonde mea-

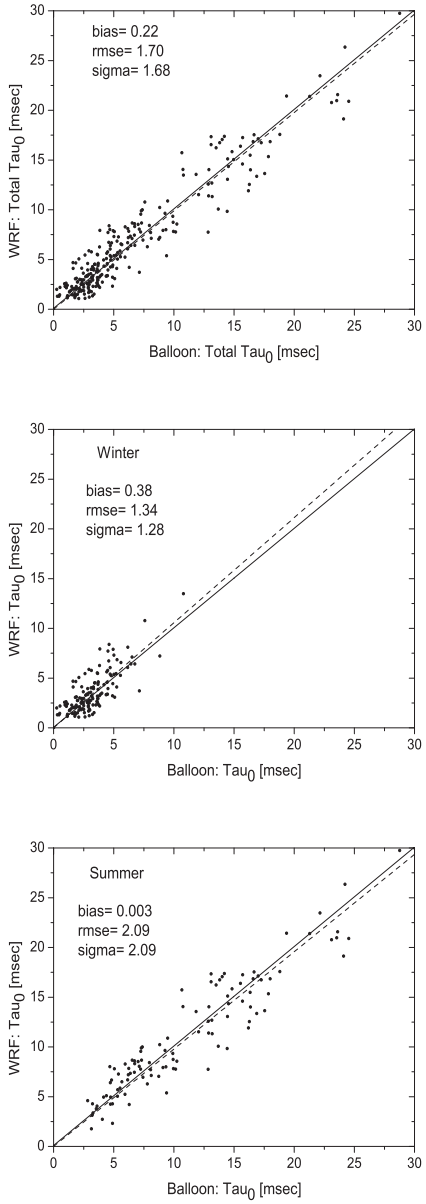

Figure 16. Scattered plots of the total τ_0 during the whole of 2016 (top), and τ_0 in the winter half-year (winter) and in the summer half-year (summer), comparing radiosonde measurements and model outputs at the Ali observatory.

surements, the results of the optical turbulence parameters derived from radiosoundings are shown as a reference, located at the Ali Meteorological Radiosonde Station (Ali-S), 4280 m above sea level, about 25 km north of the observatory. Also, the observed samples allow us to evaluate the performance of the WRF model in each season, and to statistically discuss how well the model reconstructs the optical turbulence parameters. Our main conclusions in this study are summarized as follows.

Clear seasonal variations of the C_n^2 profiles occur in the ground surface layer and the jet-stream region (12–13 km above sea level at Ali). In the free atmosphere, the values of C_n^2 are focused in the range of 10^{-18}–$10^{-13.5}$ $m^{-2/3}$. At the tropopause (12–13 km above sea level at Ali), the C_n^2 values are between $10^{-18.5}$ and $10^{-16.5}$ $m^{-2/3}$, and in summer especially, the C_n^2 is small. The vertical morphologies of C_n^2 match very well with the corresponding observed C_n^2 profiles.

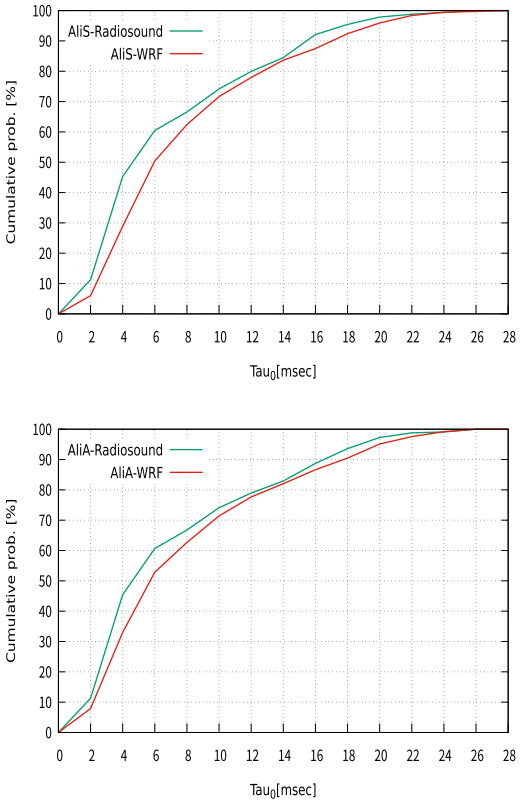

Figure 17. Cumulative probability distributions of τ_0 at night in 2016 at Ali, obtained from the radiosonde measurements (green line) and the WRF model (red line).

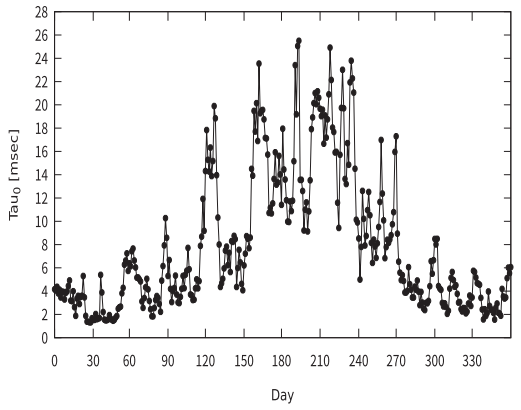

Figure 18. The daily distribution of τ_0 at night in 2016 at the Ali observatory, obtained from the WRF model.

From the model behaviour in each season, we can see the model underestimations of C_n^2 above 10 km above sea level. The bias is most likely due to the insufficient observed samples at night, only obtained at BT 07:00 (UTC 23:00), most of which are missing in summer. The small bias could be corrected, with more abundant samples. For C_n^2 in the free atmosphere, it is still difficult to reproduce extreme values and, at present, we are attempting to improve the model performance.

For the integral parameters, isoplanatic angle θ_0, seeing ε_0 and coherence time τ_0, calculated from the WRF model, these are in good agreement with the measured results. With yearly medians $\varepsilon_0 = 0.47$ arcsec, $\theta_0 = 4.35$ arcsec and $\tau_0 = 5.52$ ms in 2016

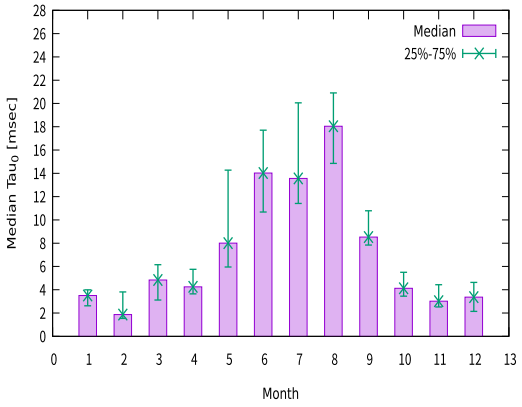

Figure 19. Monthly quartile values of τ_0 at night in 2016 at the Ali observatory, with the histograms showing the median values, and the vertical bars indicating quartile values of the τ_0.

at the Ali observatory, it is confirmed that the characteristics of optical turbulence are good, and typical of a good astronomical site in the Northern Hemisphere. Also, the atmospheric optical turbulence shows an obvious seasonal variation, with better optical turbulence conditions in summer than in winter.

In summary, the WRF model can describe the characteristics of atmospheric optical turbulence well at Ali above the west Tibetan Plateau. The detailed analysis in 2016 performed at this site shows a reliable performance with small errors with respect to the nearby radiosonde measurements for the turbulence parameters. It is found that the Ali observatory has great advantages of good optical turbulence conditions for ground-based observations, especially during the summer half-year. In future, we need to access even richer samples from different reliable measurements running at the site. This would help us to calibrate the model performance with abundant samples, and permit us to better constrain the model and quantify the uncertainty. This is especially important for improving the model performance when reconstructing the very strong and weak optical turbulence in the upper atmosphere, as well as the turbulence near the ground surface, which contributes greatly to the total integral results of optical turbulence parameters.

ACKNOWLEDGEMENTS

We acknowledge financial support from the National Natural Science Foundation of China (NSFC, Grant Nos 11973004 and 11203044). The meso-scale numerical WRF model is freely available at http://www.mmm.ucar.edu/wrf/users. Access to the ERA-Interim Reanalysis data is authorized by the ECMWF. We are also grateful to the Tianhe-2 Supercomputer System managed by the nAtional Supercomputer Center, for running the WRF model.

DATA AVAILABILITY

The observed data from radiosoundings used in this study are provided by the Ali Meteorological Bureau under licence and the data can be shared with authorization from the Ali Meteorological Bureau. The ERA-Interim reanalysis data sets for model configuration can be download from https://www.ecmwf.int/en/forecasts/datasets/reanalysis-datasets/era-interim for free.

REFERENCES

Basu S., Osborn J., He P., DeMarco A. W., 2020, MNRAS, 497, 2302B
Bougeault P., De Hui C., Fleury B., 1995, Appl. Opt., 34, 3481
Businger S., Cherubini T., 2011, Seeing Clearly: The Impact of Atmospheric Turbulence on the Propagation of Extraterrestrial Radiation. Visualbookworm.com Publishing, College Station, TX
Cherubini T., Businger S., Lyman R., 2008, J. Appl. Meteorology and Climatology, 47, 1140
Fried D. L., 1966, J. Opt. Soc. America, 56, 1372
Fried D. L., 1982, J. Opt. Soc. America, 72, 52
Giordano C., Vernin J., Vazquez Ramio H., Munoz-Tunon C., Varela A. M., Trinquet H., 2013, MNRAS, 430, 3102
Giordano C., Vernin J., Trinquet H., Munoz-Tunon C., 2014, MNRAS, 440, 1964
Hagelin S., Masciadri E., Lascaux F., 2011, MNRAS, 412, 2695
Hickson P., 2014, A&AR, 22, 76
Hickson P. et al., 2020, MNRAS, 494, 5992
Kemp E. M., Felton B. D., Allis R. J., 2008, Proc. WRF User Workshop, Estimating the Refractive Index Structure-Fuction and Related Optical Seeing Parameters with the WRF-ARW. Available at: http://citeseerx.ist.psu.edu/viewdoc/download;jsessionid=00316B372B2E0CB2F04B4F96E12AD6A3?doi=10.1.1.525.3762&rep=rep1&type=pdf
Kolmogorov A., 1941, Doklady Akademiia Nauk SSSR, 30, 301K
Li F., Wu Y., Hou Z. H., 2012, Acta Optica Sinica, 32, 0606002
Liu L. Y., Yao Y. Q., Wang Y. P., Ma J-L., He B-L., Wang H-S., 2010, Res. Astron. Astrophys., 10, 1061
Liu G. Q., Yang L., Deng L. H., Li Y. Z., Liu z., 2013, Acta Optica Sinica, 33, 0101002 [in Chinese]
Lascaux F., Masciadri E., Hagelin S., 2009, MNRAS, 398, 1093
Lascaux F., Masciadri E., Hagelin S., 2011, MNRAS, 411, 693
Masciadri E., 2003, Rev. Mex. Astron. Astrofis., 39, 249M
Masciadri E., 2006, Proc. SPIE, 6267, 62671C
Masciadri E., Vernin J., Bougeault P., 1999, A&AS, 137, 185
Masciadri E., Vernin J., Bougeault P., 2001, A&A, 365, 699
Masciadri E., Lascaux F., Fini L., 2013, MNRAS, 436, 1968
Masciadri E., Martelloni G., Turchi A., 2020, MNRAS, 492, 140
Osborn J., Sarazin M., 2018, MNRAS, 480, 1278
Qian X., Yao Y., Wang H., Wang Y., Bai Z., Yin J., 2018, PASP, 130, 125002
Qian X., Yao Y., Wang H., Zou L., Li Y., 2020a, MNRAS, 498, 5786
Qian X., Yao Y., Wang H., Zou L., Li Y., Yin J., 2020b, PASP, 132, 125003
Sarazin M. S., 1997, Proc. SPIE, 3125, 366S
Sivo G., Turchi A., Masciadri E., Guesalaga A., Neichel B., 2018, MNRAS, 476, 999S
Trinquet H., Vernin J., 2007, Environmental Fluid Mechanics, 7, 397
Turchi A., Masciadri E., Fini L., 2017, MNRAS, 466, 1943
Wang H. S., Yao Y. Q., Qian X., Liu L. Y., Wang Y. P., Li J. R., 2012, Acta Astron. Sinica, 53, 527 [in Chinese]
Wang H. S., Yao Y. Q., Liu L. Y., 2013, Acta Optica Sin., 33 ,[in Chinese]
Ye Q. Z., 2011, PASP, 123, 113

This paper has been typeset from a TEX/LATEX file prepared by the author.